

Nanocrystallization of amorphous germanium films observed with nanosecond temporal resolution

L. Nikolova,^{1,a)} T. LaGrange,^{2,b)} B. W. Reed,² M. J. Stern,³ N. D. Browning,^{2,4}
G. H. Campbell,² J.-C. Kieffer,¹ B. J. Siwick,^{3,c)} and F. Rosei^{1,5,d)}

¹*Institut National de la Recherche Scientifique, Énergie, Matériaux et Télécommunications, Varennes, Quebec J3C 1S2, Canada*

²*Physical and Life Sciences Directorate, Lawrence Livermore National Laboratory, Livermore, California 94551, USA*

³*Departments of Physics and Chemistry, Center for the Physics of Materials, McGill University, Montreal, Quebec H3A 2T8, Canada*

⁴*Department of Chemical Engineering and Materials Science and Department of Molecular and Cellular Biology, University of California-Davis, Davis, California 95616, USA*

⁵*Centre for Self-Assembled Chemical Structures, McGill University, Montreal, Quebec H3A 2K6, Canada*

(Received 26 September 2010; accepted 28 October 2010; published online 15 November 2010)

Using dynamic transmission electron microscopy we measure nucleation and growth rates during laser driven crystallization of amorphous germanium (a-Ge) films supported by silicon monoxide membranes. The films were crystallized using single 532 nm laser pulses at a fluence of $\sim 128 \text{ mJ cm}^{-2}$. Devitrification processes initiate less than 20 ns after excitation and are complete within $\sim 55 \text{ ns}$. The nucleation rate was estimated by tracking crystallite density as a function of time and reached a maximum of $\sim 1.6 \times 10^{22} \text{ nuclei/cm}^3 \text{ s}$. This study provides information on nanocrystallization phenomena in a-Ge, which is important for the implementation of nanostructured group IV semiconductors in optoelectronics devices. © 2010 American Institute of Physics. [doi:10.1063/1.3518069]

Nanostructured group IV semiconductors are promising candidate materials for use in optoelectronic devices and are typically produced through pulsed laser annealing of amorphous films. The material properties depend sensitively on the nanostructure of the film, so an understanding of the fundamentals of crystallization in amorphous semiconductors and acquisition of quantitative kinetic data under pulsed laser annealing is important.^{1,2}

Several techniques have been employed to study the crystallization behavior in amorphous silicon (a-Si) and amorphous germanium (a-Ge).^{3,4} Time-resolved optical reflectivity and transmission measurements have been used to determine the initiation of liquefaction and crystallization,⁵ but direct observation of nucleation and growth events has not been possible due to the low spatial resolution of these techniques. Since the crystallization mechanisms of laser and electron beam devitrified a-Ge and a-Si films are quite complex, nanometer spatial resolution is essential to reveal the rich microstructural phenomenology that forms over time scales ranging from a few nanoseconds to several microseconds after pulsed laser excitation.^{6–8}

The recently developed dynamic transmission electron microscope (DTEM) at LLNL permits *in situ* observation of laser induced structural transformations with $\sim 10 \text{ nm}$ spatial resolution and 15 ns temporal resolution (described in detail in Refs. 9 and 10). To achieve the high temporal resolution, two lasers are attached to the TEM column. One laser (the drive laser) induces the phase transition in the

sample and the second (cathode laser) excites a photocathode that produces a 15 ns electron pulse¹¹ via photoemission¹² that is used to form a TEM image or diffraction pattern of the laser excited area on the specimen. The crystallization process is observed by performing multiple experiments on fresh areas with different time delays set between the cathode and drive lasers, in which the temporal uncertainty between measurements taken at different time delays is defined by the timing jitter between the two laser systems, $\pm 1 \text{ ns}$. In this letter we present the results on time-resolved *in situ* nanocrystallization of a-Ge films supported by silicon monoxide (SiO) membranes using pulsed electron imaging in the DTEM. Our study aims at determining directly the crystal nucleation rate and growth velocity in laser excited a-Ge through time-resolved real-space TEM imaging of the material's microstructure.

Amorphous germanium layers of 110 nm thickness used for this study were deposited by e-beam evaporation onto commercially available 40 nm SiO films supported by 300-mesh copper grids. The amorphous nature of the Ge films was confirmed by x-ray diffraction which did not detect any long range order. The incident laser fluence was kept at 128 mJ/cm^2 , $\pm 4\%$ and time-resolved images were taken at various time delays after sample excitation ranging from 20 to 300 ns. Single-shot bright field images were acquired and analyzed to determine the number and size of nucleated grains as a function of time. The laser spot was aligned to hit the center of the field of view, allowing observation of the microstructure evolution in the middle of the crystallization zone, where the temperature of the film is the highest.

Figure 1 shows the evolution of the microstructure with time. The "0 ns" image represents the sample before laser excitation. The remaining micrographs are taken with delays between the pump and probe pulses with times denoted in

^{a)} Author to whom correspondence should be addressed. Electronic mail: nikolova@emt.inrs.ca.

^{b)} Electronic mail: lagrange2@llnl.gov.

^{c)} Electronic mail: bradley.siwick@mcgill.ca.

^{d)} Electronic mail: rosei@emt.inrs.ca.

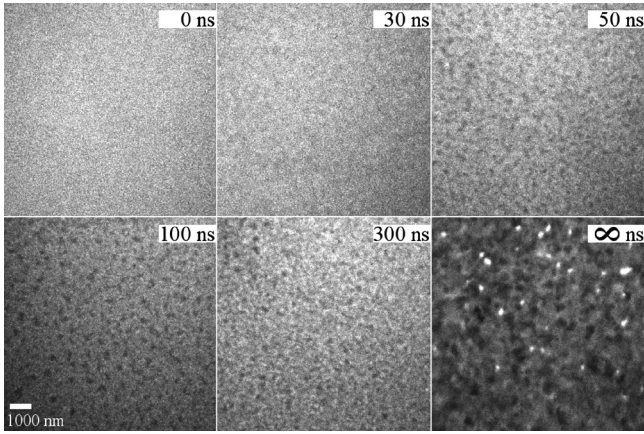


FIG. 1. Evolution of the microstructure of the a-Ge film captured at various times in independent measurements. The $\langle\langle 0 \text{ ns}\rangle\rangle$ image presents the sample structure before initiation of the transition followed by different time delays. The final image labeled $\langle\langle \infty \text{ ns}\rangle\rangle$ presents the postmortem microstructure (i.e., many seconds after cooling to ambient temperatures). The scale is the same for all the images.

the upper right corner. The final image in the bottom right corner of the figure with label “ $\infty \text{ ns}$ ” represents the final structure of the sample after cooling to room temperature. At 20 ns, crystallization has already initiated, which is consistent with prior reports using optical techniques that report the onset of crystallization 10 ns after arrival of the laser pulse.⁶ With increasing time delay, the contrast increases due to growth of the nucleated crystals resulting in larger dark features in the images. In the final structure, the film is fully crystalline and at room temperature ($\langle\langle \infty \text{ ns}\rangle\rangle$ image in Fig. 1). The white spots in the image are pores that probably form due to densification of the material or anisotropic growth and coalescence of grains similar to a previously reported crystallization behavior.^{13,7}

We quantitatively analyzed the grain size evolution with time (Fig. 2, red triangles).¹⁴ The earliest appearance of nanocrystals in the a-Ge matrix was detected at 20 ns. At this point, the crystals have an average diameter of $\sim 70 \text{ nm}$.

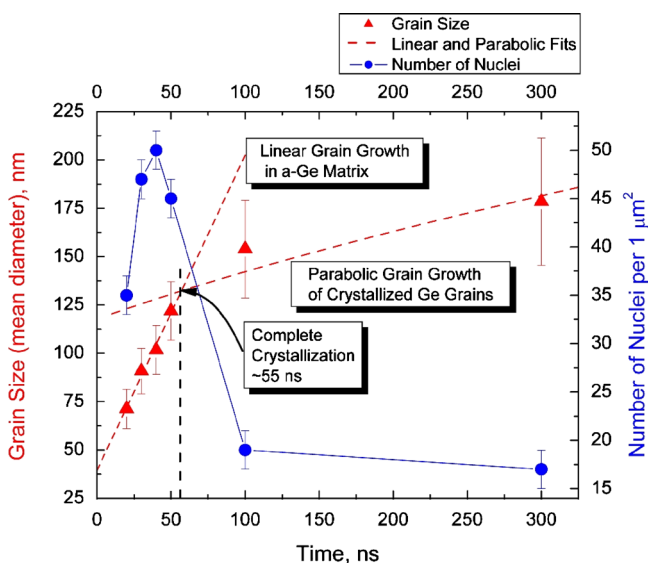


FIG. 2. (Color online) Time-resolved mean size of the crystals (red triangles) with the respective error bars. The red dashed lines present the fits for the nucleation and grain growth regions. Time-resolved number of the crystals per unit area is represented by blue disks.

Identification of individual nanocrystals at even earlier stages of devitrification was problematic due to insufficient contrast for nanocrystals $< 40 \text{ nm}$ in diameter that results from the background signal of the a-Ge film and the amorphous SiO support, the increased thermal diffuse scattering at high temperatures and the spatial superposition of smaller crystals. To obtain good statistics, the in-plane diameter of 100 crystals was taken.¹⁵ The mean grain sizes reported in Fig. 2, therefore, are an overestimate as the spatial resolution was not sufficient to observe crystals smaller than 40 nm .

The grain size initially increases linearly at time delays from 20 ns to 50 ns (Fig. 2, red dashed line), indicative of two-dimensional growth of isolated crystals during devitrification. However, for time delays greater than 50 ns the increase in grain size is parabolic, suggesting that crystallization is complete and that the grains grow preferentially by a diffusion controlled process, i.e., grains grow and coalesce by consumption of less preferred grain orientations. The intersection of the linear and parabolic fits in Fig. 2 suggests the approximate time for complete crystallization at $\sim 55 \text{ ns}$. Assuming that thermally activated crystallization follows an Arrhenius type relationship, e.g., $t = t_0 \exp(E_C/kT)$ where t is the time to fully crystallize the film, t_0 is the prefactor, E_C is the activation barrier for crystallization, k_B is Boltzmann's constant, and T is temperature, the temperature can be estimated.¹⁶ Using the data reported in Ref. 16 for the activation barrier and the prefactor (3 eV and $4 \times 10^{-17} \text{ s}$, respectively), the estimated temperature to fully crystallize the foil in 55 ns is $\sim 1700 \text{ K}$, which is far above the melting temperature (1210 K). However, melting of the film was not observed. The initial temperature rise can be estimated by noting the laser fluences required for melting (partial melting occurred at 195 mJ cm^{-2} and complete melting at 220 mJ cm^{-2}) and using this observed range to relate deposited laser energy to temperature. The heat of fusion (24 kJ mol^{-1} accounting for the amorphous-crystalline change)⁷ and the heat capacity of the SiO support were included in the calculation. Roughly, a fluence of 128 mJ cm^{-2} should heat the film to temperatures between 800 and 1050 K, corresponding to activation barriers ranging from 1.4 to 1.9 eV, assuming the same prefactor as quoted in Blum and Feldman.¹⁶ Our heating rates and temperatures are much higher than those in the calorimetric studies of Blum and Feldman, which suggest two likely explanations for the discrepancy. Either additional mechanisms become activated at higher temperatures, or the activation barrier for the same mechanism is strongly temperature dependent in a way that low-temperature measurements lack the ability to detect. Since the size and free energy of the critical nucleus depend on the volumetric free energy difference between the two phases as well as the interface free energy, both of which may vary with temperature, this explanation is plausible.

The nucleation rate was estimated by counting the number of crystals in a $1 \mu\text{m}^2$ area to determine the crystal density as a function of time (the data are summarized in Fig. 2 as blue disks on the right side Y axis). The number of crystals increased with time reaching a maximum at $\sim 40 \text{ ns}$ and decreased at times greater than 60 ns, suggesting that complete crystallization occurs within 50–60 ns and the reduction in the number of grains was due to grain growth and coalescence. Taking the discrete derivative of the data in Fig. 2, the nucleation rate N for each time delay was calculated,

with an estimated maximum of $N \approx 1.6 \times 10^{22} \text{cm}^{-3} \text{s}^{-1}$. Although this estimated nucleation rate is quite high, it is commensurate with the rapid crystallization and fine grain size, indicating that high laser fluence and temperatures near but below the melt temperature are required to produce nanocrystalline Ge films.

In summary, we report the laser induced nucleation process of a-Ge film *in situ* with nanometer spatial and nanosecond temporal resolutions. The high spatial and temporal resolutions of the dynamic TEM have permitted real-space counting of the nucleation sites and experimental determination of the density of nuclei. Future experiments will compare the nucleation rate of a-Ge supported by SiO and free-standing films and will offer additional insight into the kinetics of devitrification as the SiO support changes the heat transfer properties of the composite film and thus influences the kinetics.

L.N., J.-C.K., B.J.S., and F.R. were supported by NSERC of Canada and FQRNT and MDEIE of Quebec. T.L.G., N.B., B.W.R., and G.C. were supported through grants by the U.S. Department of Energy, Office of Basic Energy Sciences, Division of Materials Sciences and Engineering and work was performed under the auspices of the U.S. Department of Energy by LLNL under Contract No. DE-AC52-07NA27344. B.J.S., J.-C.K., and F.R. acknowledge partial salary support from the Canada Research Chairs program. L.N. acknowledges CGS Alexander Graham Bell from NSERC and FQRNT for postgraduate fellowships.

- ¹M. L. Taheri, S. McGowan, L. Nikolova, J. E. Evans, N. Teslich, J. P. Lu, T. LaGrange, F. Rosei, B. J. Siwick, and N. D. Browning, *Appl. Phys. Lett.* **97**, 032102 (2010).
- ²M. I. Ortiz, A. Rodriguez, J. Sangrador, T. Rodriguez, M. Avella, J. Jimenez, and C. Ballesteros, *Nanotechnology* **16**, S197 (2005).
- ³M. Lee, S. Moon, and C. P. Grigoropoulos, *J. Cryst. Growth* **226**, 8 (2001).
- ⁴C.-C. Kuo, W.-C. Yeh, J.-B. Chen, and J.-Y. Jeng, *Thin Solid Films* **515**, 1651 (2006).
- ⁵C.-C. Kuo, W.-C. Yeh, J.-F. Lee, and J.-Y. Jeng, *J. Phys.: Conf. Ser.* **48**, 937 (2006).
- ⁶O. Bostanjoglo, W. Marine, and P. Thomsen-Schmidt, *Appl. Surf. Sci.* **54**, 302 (1992).
- ⁷R. K. Sharma, S. K. Bansal, R. Nath, and R. M. Mehra, *J. Appl. Phys.* **55**, 387 (1984).
- ⁸O. Bostanjoglo, *Phys. Status Solidi A* **70**, 473 (1982).
- ⁹T. Lagrange, G. H. Campbell, B. W. Reed, M. Taheri, J. B. Pesavento, J. S. Kim, and N. D. Browning, *Ultramicroscopy* **108**, 1441 (2008).
- ¹⁰B. W. Reed, M. R. Armstrong, N. D. Browning, G. H. Campbell, J. E. Evans, T. LaGrange, and D. J. Masiel, *Microsc. Microanal.* **15**, 272 (2009).
- ¹¹The effective exposure time of the images and diffraction patterns is the electron pulse duration.
- ¹²The conventional thermionic electron gun was replaced by a photocathode.
- ¹³H. J. Leamy, W. L. Brown, G. K. Celler, G. Foti, G. H. Gilmer, and J. C. C. Fan, *Laser and Electron-Beam Solid Interactions and Materials Processing*, MRS Symposia Proceedings (Materials Research Society, Warrendale, 1980), Vol. 1, p. 89.
- ¹⁴Grain size measurements were made manually.
- ¹⁵The reported diameters are the mean values from 100 crystals, which are identified as contiguous regions in the image of at least nine pixels with a central gray level as least 20% darker than that of the surrounding amorphous material.
- ¹⁶N. A. Blum and C. Feldman, *J. Non-Cryst. Solids* **22**, 29 (1976).